

Article

Single Crystal Elastic Properties of Hemimorphite, a Novel Hydrous Silicate

Yingzhe Li and Jay D. Bass *

Geology Department, University of Illinois, Urbana, IL 61801, USA; yli200@illinois.edu

* Correspondence: jaybass@illinois.edu; Tel.: +1-217-333-1018

Received: 6 April 2020; Accepted: 7 May 2020; Published: 10 May 2020



Abstract: Hemimorphite, with the chemical formula $Zn_4Si_2O_7(OH)_2 \cdot H_2O$, contains two different types of structurally bound hydrogen: molecular water and hydroxyl. The elastic properties of single-crystal hemimorphite have been determined by Brillouin spectroscopy at ambient conditions, yielding tight constraints on all nine single-crystal elastic moduli (C_{ij}). The Voigt–Reuss–Hill (VRH) averaged isotropic aggregate elastic moduli are K_S (VRH) = 74(3) GPa and μ (VRH) = 27(2) GPa, for the adiabatic bulk modulus and shear modulus, respectively. The average of the Hashin–Shtrickman (HS) bounds are K_S (HS) = 74.2(7) GPa and μ (HS) = 26.5(6) GPa. Hemimorphite displays a high degree of velocity anisotropy. As a result, differences between upper and lower bounds on aggregate properties are large and the main source of uncertainty in K_S and μ . The HS average P wave velocity is $V_P = 5.61(4)$ km/s, and the HS S-wave velocity is $V_S = 2.77(3)$ km/s. The high degree of elastic anisotropy among the on-diagonal longitudinal and pure shear moduli of hemimorphite are largely explained by its distinctive crystal structure.

Keywords: elastic properties; Brillouin; hydrogen bonds; sound velocity

1. Introduction

The influence of hydrogen, or “water”, on the elastic properties of minerals is a topic of great current interest for possibly identifying hydrous phases in the deep crust and mantle from seismic models for these regions. Adding hydrogen bonds into crystal structures is widely assumed to decrease the density, and elastic moduli of silicate minerals by increasing their volume, at least at ambient conditions. However, the effect of water on the elastic properties of minerals can depend greatly on details of the crystal structure into which hydrogen is incorporated, and on whether hydrogen is present in the form of hydroxyl OH^- or as molecular water. Hydration of wadsleyite, ringwoodite and garnet can change elastic moduli significantly [1,2], in contrast to the olivine-chondrodite group [3], which varies less, with a similar water content. These differences are considered to be caused by different incorporation mechanisms of hydrogen into their structures. To investigate the influence of water on the direction-dependent compressibility, or elastic anisotropy, of minerals, it is necessary to measure the single-crystal elastic moduli matrix, C_{ij} . Hemimorphite, $Zn_4Si_2O_7(OH)_2 \cdot H_2O$, a hydrated alteration product of willemite, Zn_2SiO_4 , is interesting, in that it contains both molecular H_2O and OH^- hydroxyl bonded into its structure. In nature hemimorphite is an economic ore mineral in supergene non-sulfide zinc deposits. Some significant deposits are dominated by hemimorphite, such as Shaimerden supergene deposit in Kazakhstan, the Cho Dien district in Vietnam, and the Skorpion deposit in Namibia [4].

The content of structurally bound H_2O of hemimorphite is 7.18 wt% [5]. It has two phase transitions below room temperature related to ordered versus dynamically disordered H_2O and OH^- in the crystal structure at 20 and 90 K, respectively [6]. At elevated temperatures, hemimorphite dehydrates in two stages. It loses molecular H_2O without breakdown of the structure at 550 °C, then

undergoes a phase transition to β - Zn_2SiO_4 , involving release of the OH^- group between 725–760 °C. If heated above 960 °C, it transforms into willemite (α - Zn_2SiO_4) [7].

The structure of orthorhombic hemimorphite, with space group $Imm2$, is composed of a three-dimensional framework, in which two $\text{ZnO}_3(\text{OH})$ tetrahedra and one SiO_4 tetrahedron form three-membered rings that are corner-shared to form corrugated sheets parallel to (010) [8,9] (Figure 1). SiO_4 tetrahedra in one layer are linked to SiO_4 tetrahedra in an adjacent layer, while the $\text{ZnO}_3(\text{OH})$ tetrahedra in adjacent layers also only link to each other, completing the framework. Large open channels run parallel to [001], giving hemimorphite a structural similarity to zeolites. The molecular water, orientated in the (010) plane, is near the center of large cavities of an eight-membered ring and bonded to hydroxyl groups of the $\text{ZnO}_3(\text{OH})$ tetrahedra by hydrogen bonds. The hydrogen bonds formed by H of hydroxyl group (H35) are stronger than those formed by H of molecular water (H53) [8]. The presence of both hydroxyl and molecular water, corrugated sheets in a tetrahedral framework, and large zeolitic cavities, make hemimorphite a rather novel silicate mineral. The objective of this project was to measure the elastic properties of hemimorphite, in order to investigate its structure-property relations, and as a first step toward understanding how H_2O and OH^- influence sound velocities and elasticity.

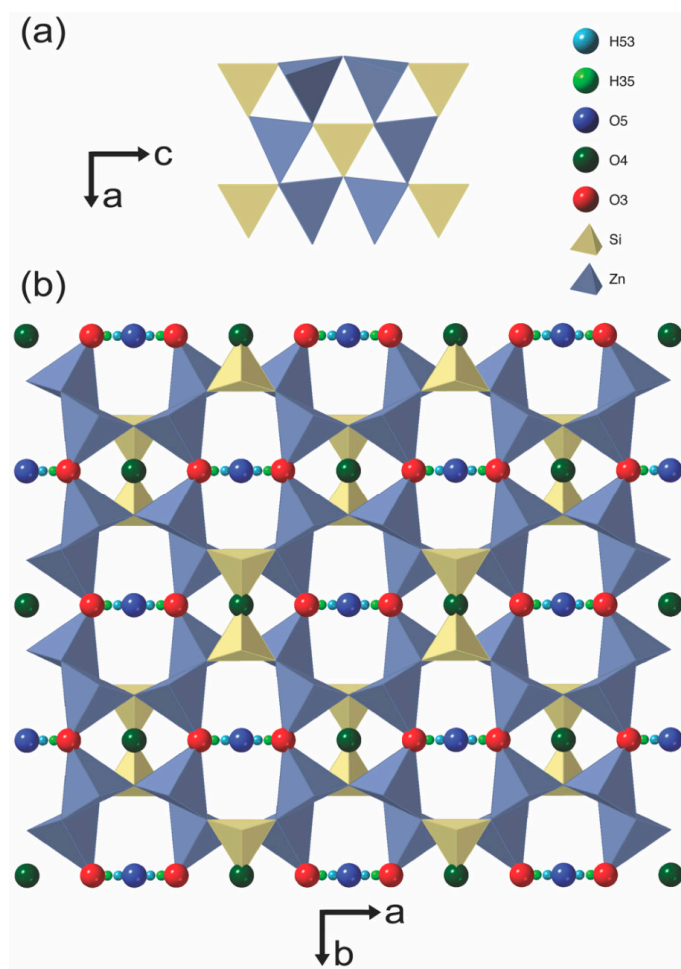


Figure 1. The crystal structure of hemimorphite. (a) Here, two zinc and one silicon tetrahedra comprise three-membered ring in (010) plane; (b) the structure of hemimorphite projected onto the a–b plane. Six-membered rings and eight-membered rings are in the a–b plane. Large cavities run along the c axis and contain H_2O . The corrugated layers of three-membered rings are also apparent in this projection (modified from Hill, et al., 1977 [8]).

2. Materials and Methods

Our samples of hemimorphite are from the Mapimí mine, Durango, Mexico. The sample contains a “spray” of transparent euhedral crystals with clearly defined faces. Most crystals exhibit tabular planes parallel to (010), and striations parallel to [001]. From single-crystal X-ray diffraction using a four-circle diffractometer, the average lattice parameters obtained on three single crystals are: $a = 8.37(2) \text{ \AA}$, $b = 10.722(4) \text{ \AA}$, and $c = 5.118(7) \text{ \AA}$, with unit cell volume $V_0 = 459(1) \text{ \AA}^3$. The lattice parameters are consistent with the values reported in earlier crystal structure determinations by Hill et al. [8], McDonald and Cruickshank [9], Takeuchi et al. [10] and Cooper and Gibbs [11].

Scanning electron microscopy-energy dispersive spectroscopy (SEM-EDS) was used to obtain the major element chemical composition of hemimorphite. The results show that our samples are iron-free, nearly pure zinc silicates. The calculated density $\rho = 3.48 (3) \text{ g/cm}^3$ was derived from the chemical formula $\text{Zn}_4\text{Si}_2\text{O}_7(\text{OH})_2 \cdot \text{H}_2\text{O}$ with $Z = 2$ and the unit cell volume given by X-ray diffraction.

Three near-principal sections of hemimorphite were polished with parallel faces in the a–b, b–c, and a–c crystallographic planes. The orientations of the polished surfaces were obtained by specular goniometry measurements and the X-ray orientation matrices for each crystal. The accuracy of sample orientation was within 0.5 degrees. For the Brillouin scattering measurements, a single-frequency diode pumped solid-state laser of wavelength 532 nm was used as a light source. All measurements were performed using a 90° platelet symmetric scattering geometry [12] at ambient conditions. The scattered light was analyzed by a piezoelectrically-scanned tandem Fabry–Perot interferometer [13].

For each principal section, acoustic velocities were determined in 26 distinct crystallographic directions by changing the chi angle on the three-circle Eulerian cradle in 15 degree increments. Measurements were made in a total of 78 distinct crystallographic directions, yielding 156 acoustic mode velocities (78 longitudinal and 78 single shear modes).

3. Results

From the measured Brillouin frequency shifts, $\Delta\nu_B$, velocity v in a given crystallographic direction i is derived from the equation for symmetric platelet geometry [12]:

$$v_i = \frac{\lambda_0 \Delta\nu_B}{2 \sin \frac{\theta}{2}} \quad (1)$$

where λ_0 is the wavelength of the incident laser light, and θ is the external angle between the incident and scattered light.

The single-crystal elastic moduli tensor of orthorhombic hemimorphite contains nine independent non-zero elastic moduli C_{ij} . On-diagonal moduli were well constrained by the acoustic velocities in the directions very close to the crystallographic axes. A linearized inversion method of Weidner and Carleton [14], was used to obtain a least-squares best-fit model of the elastic moduli C_{ij} derived from the velocities. Figure 2 and Table 1 show a comparison between model and observed data of phonon velocities. The root-mean-square (RMS) residual in velocity for the final best-fit C_{ij} model is 32.4 m/s. Hemimorphite exhibits considerable longitudinal and shear velocity anisotropy (Figure 2 and Table 2).

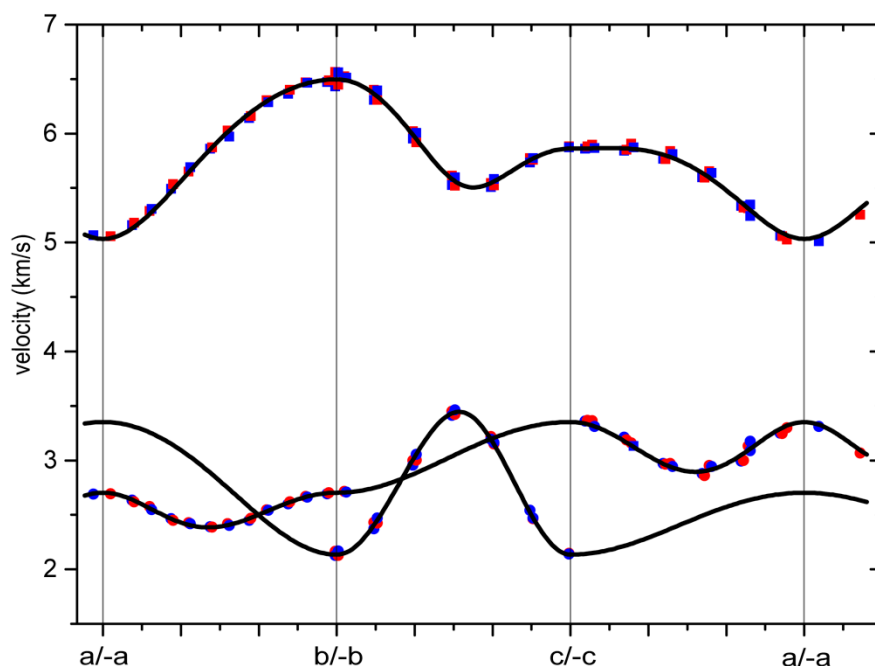


Figure 2. Measured acoustic velocities of hemimorphite (solid symbols), as a function of crystallographic directions projected onto the a–b, b–c, and a–c crystallographic planes. Squares and circles represent V_P and V_S measurements, respectively. The red symbols are measured on (001), (100) and (010); blue symbols are measured on the (001̄), (00) and (010). The best-fit acoustic velocity model is shown by solid lines. Error bars are smaller than the size of symbols.

Table 1. Acoustic measurements of hemimorphite at ambient conditions.

Phonon Direction Cosines			V_P (m/s)			V_S (m/s)		
n_a	n_b	n_c	Obs.	Model	Residual	Obs.	Model	Residual
0.936	−0.005	−0.352	5314	5293	21	3130	3110	20
0.812	−0.009	−0.583	5654	5580	73	2951	2916	35
0.632	−0.013	−0.775	5837	5777	60	2971	2935	36
0.409	−0.016	−0.912	5906	5858	48	3159	3126	33
0.159	−0.016	−0.987	5897	5865	33	3362	3314	48
−0.102	−0.012	−0.995	5881	5863	18	3367	3337	31
−0.355	−0.004	−0.935	5851	5864	−12	3188	3176	12
−0.584	0.006	−0.812	5764	5806	−42	2964	2969	−5
−0.773	0.016	−0.634	5594	5640	−46	2861	2900	−39
−0.91	0.024	−0.414	5318	5371	−53	2998	3048	−50
−0.986	0.028	−0.167	5057	5103	−47	3246	3286	−40
−0.995	0.027	0.092	5027	5057	−31	3299	3331	−31
−0.938	0.021	0.345	5253	5286	−33	3066	3118	−52
−0.942	0.001	0.336	5241	5275	−34	3089	3126	−37
−0.997	0.000	0.083	5011	5051	−40	3312	3335	−23
−0.985	0.003	−0.176	5063	5109	−46	3248	3279	−31
−0.906	0.008	−0.423	5334	5381	−47	2991	3038	−48
−0.767	0.015	−0.641	5596	5647	−51	2878	2898	−20
−0.576	0.022	−0.817	5766	5809	−43	2972	2975	−3
−0.346	0.027	−0.938	5840	5863	−24	3212	3183	28
−0.092	0.027	−0.995	5859	5862	−3	3361	3339	22
0.169	0.023	−0.985	5867	5864	4	3312	3309	4
0.418	0.014	−0.908	5873	5857	16	3133	3118	15
0.64	0.003	−0.769	5811	5773	38	2944	2930	14

Table 1. Cont.

Phonon Direction Cosines			V _P (m/s)			V _S (m/s)		
n _a	n _b	n _c	Obs.	Model	Residual	Obs.	Model	Residual
0.817	−0.008	−0.576	5637	5571	65	2943	2920	24
0.939	−0.018	−0.343	5348	5283	64	3175	3120	55
0.004	−1.000	0.003	6446	6497	−51	2126	2136	−10
0.007	−0.965	0.261	6308	6349	−42	2425	2434	−9
0.012	−0.865	0.501	5920	5965	−46	3003	3037	−34
0.018	−0.707	0.708	5521	5570	−49	3422	3438	−16
0.022	−0.500	0.866	5524	5555	−30	3150	3163	−14
0.024	−0.259	0.966	5757	5764	−6	2465	2497	−33
0.022	0.000	1.000	5880	5862	18	2146	2136	10
0.017	0.259	0.966	5772	5763	9	2540	2498	42
0.008	0.500	0.866	5545	5554	−9	3218	3169	49
−0.003	0.708	0.706	5612	5572	41	3451	3437	14
−0.013	0.867	0.499	6020	5971	49	2999	3030	−31
−0.021	0.966	0.256	6400	6354	46	2429	2425	4
−0.025	1.000	−0.003	6563	6497	67	2164	2137	27
−0.008	1.000	0.006	6562	6497	64	2166	2136	29
−0.007	0.964	0.265	6393	6345	49	2471	2443	28
−0.009	0.862	0.506	6004	5954	49	3053	3050	2
−0.012	0.701	0.713	5596	5563	33	3462	3441	21
−0.014	0.492	0.870	5582	5560	22	3163	3148	15
−0.013	0.250	0.968	5774	5770	4	2469	2475	−6
−0.01	−0.010	1.000	5872	5862	10	2140	2137	3
−0.003	−0.268	0.964	5732	5757	−25	2541	2520	20
0.005	−0.508	0.862	5509	5548	−39	3193	3188	5
0.015	−0.713	0.701	5527	5579	−52	3412	3433	−22
0.023	−0.870	0.493	5954	5981	−27	2956	3017	−61
0.028	−0.967	0.252	6309	6359	−50	2372	2416	−44
0.029	−1.000	−0.006	6433	6497	−64	2126	2138	−11
0.029	−0.999	0.034	6524	6494	30	2713	2703	10
−0.228	−0.973	0.041	6470	6445	25	2667	2658	9
−0.469	−0.882	0.047	6306	6276	30	2543	2541	2
−0.68	−0.732	0.049	6028	5992	36	2418	2396	23
−0.845	−0.533	0.048	5651	5623	29	2427	2409	18
−0.954	−0.298	0.045	5288	5250	38	2575	2566	9
−0.998	−0.042	0.040	5055	5042	13	2694	2699	−5
−0.975	0.218	0.033	5179	5155	24	2617	2624	−7
−0.886	0.464	0.025	5534	5502	32	2449	2449	−1
−0.735	0.678	0.015	5871	5891	−20	2387	2387	0
−0.533	0.846	0.005	6161	6211	−50	2467	2481	−14
−0.294	0.956	−0.005	6400	6417	−17	2618	2626	−8
−0.033	0.999	−0.014	6488	6495	−8	2701	2702	−1
−0.043	0.998	−0.036	6471	6492	−21	2692	2703	−11
−0.303	0.953	−0.025	6364	6410	−46	2600	2622	−22
−0.541	0.841	−0.013	6142	6200	−58	2448	2474	−26
−0.742	0.671	−0.001	5860	5878	−18	2389	2387	2
−0.89	0.455	0.011	5493	5488	6	2465	2455	9
−0.978	0.209	0.021	5157	5145	12	2633	2630	3
−0.998	−0.051	0.029	5066	5042	24	2690	2698	−8
−0.951	−0.306	0.034	5309	5261	48	2549	2561	−12
−0.84	−0.541	0.036	5691	5637	54	2419	2407	12
−0.674	−0.738	0.035	5971	6005	−34	2401	2401	0
−0.462	−0.886	0.031	6287	6286	1	2541	2534	7
−0.22	−0.975	0.024	6466	6451	14	2663	2660	3
0.037	−0.999	0.016	6512	6495	17	2708	2702	5

Table 2. Direction of maximum and minimum V_P and V_S .

	Vel (km/s)	Phonon Direction Cosines		
Max V_P	6.497	0	1	0
Min V_P	5.033	1	0	0
Max V_S	3.446	0	−0.682	0.731
Min V_S	2.136	0	1	0

Using the inversion method of Brown [15], we obtained virtually identical results for the C_{ij} and their 1σ uncertainties. Table 3 shows the resulting C_{ij} values for hemimorphite. We note the large differences among the moduli C_{11} , C_{22} , and C_{33} , with C_{11} 40% smaller than C_{22} , are a result of the large acoustic anisotropy of hemimorphite.

Table 3. Single-crystal elastic moduli of hemimorphite (GPa).

C_{11}	C_{22}	C_{33}	C_{44}	C_{55}	C_{66}	C_{12}	C_{13}	C_{23}
88.2(4)	147.0(4)	119.7(4)	15.9(1)	39.1(2)	25.5(2)	73.5(4)	43.9(4)	49.6(5)

From the single-crystal moduli, the Voigt, Reuss, and Hashin–Shtrikman bounds on the adiabatic bulk modulus K_S , and shear modulus μ of an isotropic aggregate were calculated, along with the Hill (Voigt–Reuss–Hill (VRH)) averages (Table 4). The Voigt and Reuss bounds on the bulk modulus and shear modulus differ by factors of 7% and 17%, respectively. The differences are due to the moderately strong anisotropy for both longitudinal waves and shear waves. We note that the Hill average is within the range of the Hashin–Shtrikman bounds.

Table 4. Isotropic aggregate elastic properties of hemimorphite.

Aggregate Properties	Voigt	Reuss	Hill (Voigt–Reuss–Hill (VRH)) Averages	Hashin–Shtrikman Bounds
Bulk modulus, K_S , GPa	76.5(2)	71.3(3)	74(3)	73.6(1)–74.8(1)
Shear modulus, μ , GPa	28.63(6)	24.42(6)	27(2)	26.05 (6)–27.04(6)
V_P , km/s	5.74(1)	5.46(1)	5.6(1)	5.58(1)–5.64(1)
V_S , km/s	2.87(1)	2.65(1)	2.8(1)	2.74(1)–2.79(1)
Density, g/cm^3	3.48(3)			

From the values of K_S (VRH) and μ (VRH), the sound velocities appropriate to an isotropic polycrystalline aggregate were calculated to be $V_{P,agg} = \sqrt{\left(\frac{K+\frac{4}{3}\mu}{\rho}\right)} = 5.6(1)$ km/s; $V_{S,agg} = \sqrt{\left(\frac{\mu}{\rho}\right)} = 2.8(1)$ km/s (Table 4). The longitudinal and shear velocity anisotropy are defined as $(V_{P,maximum} - V_{P,minimum})/V_{P,(VRH)} = 26\%$ and $(V_{S,maximum} - V_{S,minimum})/V_{S,(VRH)} = 47\%$, respectively.

Seryotkin et al. [16] studied the structural changes of hemimorphite at pressures up to 4.2 GPa by X-ray diffraction and the diamond-anvil cell. The purpose of their study was to search for a high-pressure phase transition, which they found near 2.5 GPa. We fitted their data on hemimorphite to a 2nd-order Birch Murnaghan equation of state and obtain $K_T = 70(6)$ GPa (K_T' assumed to be 4), in agreement with our result of $K_S = 74(3)$. Their experiments also show that the a-axis of hemimorphite is most compressible, while the b-axis is most rigid, in agreement with our result $C_{22} > C_{33} > C_{11}$. For the purpose of comparing our results and static compression results, we have ignored the difference between the adiabatic and isothermal bulk modulus, which is typically $\sim 1\%$.

Interestingly, we note that our value of K_S for hemimorphite is in excellent agreement with the value of $K_T = 72(2)$ GPa for bertrandite, $\text{Be}_4\text{Si}_2\text{O}_7(\text{OH})_2$, measured by Hazen and Au [17]. Bertrandite is topologically identical to hemimorphite, but differs chemically and does not contain molecular water in the large open cavities of the structure. The fact that bertrandite and hemimorphite have the same bulk modulus, despite having significant chemical differences, likely indicates a dominant influence of

crystal-structural topology on the physical properties of these materials. However, it is also possible that the substitution of Zn for Be, and the presence of H₂O in hemimorphite, have opposite but equal effects on the bulk modulus that nearly cancel. There is some evidence to support this possibility. The Zn–O bond is longer than the Be–O bond and the bulk modulus of the BeO₄ tetrahedron is significantly larger than that of the ZnO₄ tetrahedron [18]. On the other hand, Cooper and Gibbs [11] found that upon dehydrating H₂O from the structure, the large cavities contract. This may suggest that H₂O provides support for the structure and stiffens it. It would be interesting to test this possibility on dehydrated hemimorphite, which would shed light on the effect of molecular water on this structure.

4. Discussion

The compressibility of minerals depends on the compressibility of the constituent cation polyhedra and their linkages to each other via angle-bending forces [17,18]. In their high-pressure X-ray structural study of bertrandite, Be₄Si₂O₇(OH)₂, which is structurally identical to hemimorphite Hazen and Au [17], concluded that polyhedral rotation and angle bending were the main compression mechanisms, as opposed to compression of tetrahedra. This is supported by the fact that the bulk modulus of bertrandite, 70(3) GPa, is much smaller than the polyhedral bulk moduli of the BeO₄ and SiO₄ tetrahedra (~200 GPa for both [17]). As noted above, our result for the bulk modulus of hemimorphite is identical to K_T measured by Hazen and Au [17], providing additional support for this interpretation.

The C_{ij} tensor of hemimorphite shows that strong anisotropy is a distinctive property of this mineral. We believe that this high degree of anisotropy is largely due to the topology of the hemimorphite crystal structure. C₁₁ and C₃₃ are the compressional moduli acting parallel to the corrugated sheets of tetrahedra. C₁₁ is a measure of the stiffness in the a direction, normal to the corrugations in the tetrahedral sheets (Figure 3). Strain in this direction can be accommodated by a high degree of angle bending of the corrugations in an accordion-like fashion, and with little or no strain of the tetrahedra themselves. Thus, the value of C₁₁ is the lowest of the three compressional moduli.

The strongest elements in the hemimorphite crystal structure are the Si₂O₇ groups that bond across the apical oxygens in adjacent (010) layers. The structure cannot be compressed along [010] without some strain being accommodated by the Si tetrahedra, which are the strongest polyhedra [18]. The Si₂O₇ groups are essentially rigid pylons that stiffen the structure in the [010] direction. Thus, we attribute C₂₂ being the largest longitudinal modulus of hemimorphite as being largely due to the Si₂O₇ groups. This situation is reminiscent of the olivine structure, in which SiO₄ tetrahedra are contained in columns along the a direction, yielding C₁₁ as the largest longitudinal modulus [19].

C₅₅ is the largest of the on-diagonal pure-shear moduli. The C₅₅ modulus corresponds to shear within the (010) plane, parallel to the tetrahedral sheets. These corrugated sheets contain only 3-membered rings of Zn and Si tetrahedra. There is virtually no rotational freedom or angle-bending for 3-membered rings in response to a shear stress within their tetrahedral basal planes. Strain within the tetrahedral sheets must be accommodated by either shearing of the tetrahedra themselves, or perhaps the tilting of tetrahedra out of the basal plane. This gives the structure high shear rigidity within the plane of a tetrahedral sheet. In support of this interpretation, we look to mica, which has tetrahedral sheets within the a-b plane, parallel to (001). The shear modulus corresponding to this tetrahedral sheet is C₆₆ = 72 GPa [20]. In comparison, the other shear moduli are far smaller, with C₄₄ = 16.5 GPa and C₅₅ = 19.5 GPa. In the cases of both hemimorphite and muscovite, the polyhedral topology, in particular tetrahedral sheets, dictates which of the pure shear moduli is largest. We suggest that the tetrahedral sheets in hemimorphite are less rigid than those in muscovite, for two reasons. Firstly, in hemimorphite, only 1/3 of the tetrahedra are SiO₄, the strongest tetrahedral unit [18], whereas in muscovite, all the tetrahedra are SiO₄ in composition. Secondly, in muscovite the sheets are planar, whereas in hemimorphite the sheets are corrugated and exhibit some tilting of tetrahedra out of the (010) plane. Both the structural and chemical heterogeneity of hemimorphite make the rigidity of the tetrahedral sheets less than those in muscovite.

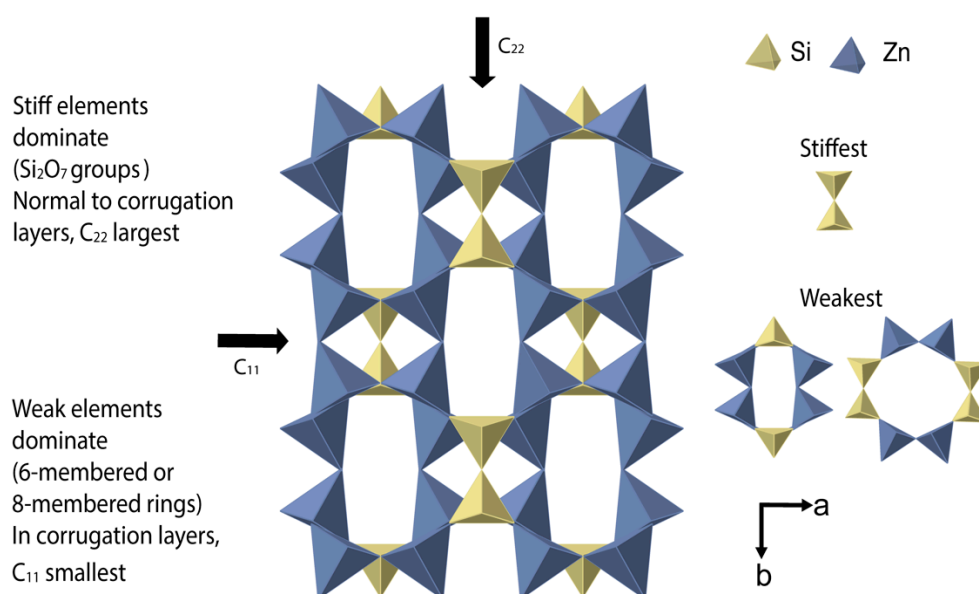


Figure 3. Schematic illustration of a polyhedral model of mineral elasticity. Hydrogens in molecular water and hydroxyls are omitted to emphasize linkages among Si and Zn tetrahedra into corrugated sheets of 3-membered rings parallel to (010), and the bridging between sheets. Stiffness parallel to [010], normal to the sheets, depends on the strongest structural element in this direction, which are Si₂O₇ and Zn₂O₆(OH)₂ groups that bridge the sheets along b. Within the plane of the sheets, the moduli depend on the weakest structural elements [19]. C₁₁, measuring stiffness in the a direction, depends, in part, on the stiffness of relatively weak 6-membered and 8-membered rings, which can accommodate strain along [100].

5. Conclusions

The nine single-crystal elastic moduli of hemimorphite have been measured at ambient conditions. The relative magnitudes of the longitudinal elastic moduli, $C_{22} > C_{33} > C_{11}$, can be qualitatively explained by the topology of the hemimorphite crystal structure. Strong Si₂O₇ groups greatly stiffen the structure along [010]. For the pure shear moduli, C₅₅ is the largest, due to the lack of rotational freedom of Zn and Si within three-membered rings in sheets parallel to (010). The elastic character of hemimorphite is largely determined by the topology of the crystal structure.

Author Contributions: Conceptualization, J.D.B.; methodology, J.D.B. and Y.L.; software, Y.L.; formal analysis, J.D.B. and Y.L.; investigation, formal analysis, J.D.B. and Y.L.; resources, J.D.B.; data curation, Y.L. and J.D.B.; writing—original draft preparation Y.L.; writing—review and editing, J.D.B.; visualization, Y.L.; supervision, J.D.B.; project administration, J.D.B.; funding acquisition, J.D.B. All authors have read and agreed to the published version of the manuscript.

Funding: This research was supported by the National Science Foundation, under grant EAR 16-20616.

Acknowledgments: The authors thank Jin S. Zhang for helpful suggestions and Paul Ginsberg for help with data analysis. We thank two anonymous reviewers, whose comments and suggestions improved the manuscript.

Conflicts of Interest: The authors declare no conflict of interest.

References

1. Wang, J.; Sinogeikin, S.V.; Inoue, T.; Bass, J.D. Elastic properties of hydrous ringwoodite. *Am. Mineral.* **2003**, *88*, 1608–1611. [[CrossRef](#)]
2. O'Neill, B.; Bass, J.D.; Rossman, G.R. Elastic properties of hydrogrossular garnet and implications for water in the upper mantle. *J. Geophys. Res. Solid Earth* **1993**, *98*, 20031–20037. [[CrossRef](#)]
3. Sinogeikin, S.V.; Bass, J.D. Single-crystal elastic properties of chondrodite: Implications for water in the upper mantle. *Phys. Chem. Miner.* **1999**, *26*, 297–303. [[CrossRef](#)]

4. Hitzman, M.W.; Reynolds, N.A.; Sangster, D.F.; Allen, C.R.; Carman, C.E. Classification, genesis, and exploration guides for non-sulfide zinc deposits. *Econ. Geol. Bull. Soc.* **2003**, *98*, 685–714. [[CrossRef](#)]
5. Bissengaliyeva, M.R.; Bekturganov, N.S.; Gogol, D.B. Thermodynamic characteristics of a natural zinc silicate hemimorphite. *J. Therm. Anal. Calorim.* **2010**, *101*, 49–58. [[CrossRef](#)]
6. Kolesov, B. Raman investigation of H₂O molecule and hydroxyl groups in the channels of hemimorphite. *Am. Mineral.* **2006**, *91*, 1355–1362. [[CrossRef](#)]
7. Taylor, H.F.W. The dehydration of hemimorphite. *Am. Mineral.* **1962**, *47*, 932–944.
8. Hill, R.J.; Gibbs, G.V.; Craig, J.R.; Ross, F.K.; Williams, J.M. A neutron-diffraction study of hemimorphite. *Z. Kristallogr.* **1977**, *146*, 241–259. [[CrossRef](#)]
9. McDonald, W.S.; Cruickshank, D.W.J. Refinement of the structure of hemimorphite. *Z. Kristallogr.* **1967**, *124*, 180–191. [[CrossRef](#)]
10. Takeuchi, Y.; Sasaki, S.; Joswig, W.; Fuess, H. X-ray and neutron diffraction study of hemimorphite. *Proc. Jpn. Acad.* **1978**, *54*, 577–582. [[CrossRef](#)]
11. Cooper, B.J.; Gibbs, G.V. The effect of heating and dehydration on the crystal structure of hemimorphite up to 600 °C. *Z. Kristallogr.* **1981**, *146*, 241–259.
12. Whitfield, C.H.; Brody, E.M.; Bassett, W.A. Elastic moduli of NaCl by Brillouin scattering at high pressure in a diamond anvil cell. *Rev. Sci. Instrum.* **1976**, *47*, 942–947. [[CrossRef](#)]
13. Loudon, R.; Sandercock, J.R. Analysis of the light-scattering cross section for surface ripples on solids. *J. Phys. C Solid State Phys.* **1980**, *13*, 2609–2622. [[CrossRef](#)]
14. Weidner, D.J.; Carleton, H.R. Elasticity of coesite. *J. Geophys. Res.* **1977**, *82*, 1334–1346. [[CrossRef](#)]
15. Brown, J.M. Determination of elastic moduli from measured acoustic velocities. *Ultrasonics* **2018**, *90*, 23–31. [[CrossRef](#)] [[PubMed](#)]
16. Seryotkin, Y.V.; Bakakin, V.V. Structural evolution of hemimorphite at high pressure up to 4.2 GPa. *Phys. Chem. Miner.* **2011**, *38*, 679–684. [[CrossRef](#)]
17. Hazen, R.M.; Au, A.Y. High-pressure crystal-chemistry of phenakite (Be₂SiO₄) and bertrandite (Be₄Si₂O₇(OH)₂). *Phys. Chem. Miner.* **1986**, *13*, 69–78. [[CrossRef](#)]
18. Hazen, R.M.; Finger, L.W. Bulk modulus-volume relationship for cation-anion polyhedra. *J. Geophys. Res. Solid Earth* **1979**, *84*, 6723–6728. [[CrossRef](#)]
19. Bass, J.D.; Weidner, D.J.; Hamaya, N.; Ozima, M.; Akimoto, S. Elasticity of the olivine and spinel polymorphs of Ni₂SiO₄. *Phys. Chem. Miner.* **1984**, *10*, 261–272. [[CrossRef](#)]
20. Vaughan, M.T.; Guggenheim, S. Elasticity of muscovite and its relationship to crystal structure. *J. Geophys. Res. Solid Earth* **1986**, *91*, 4657–4664. [[CrossRef](#)]

